GD2-Targeting CAR T-cell Therapy for Patients with GD2+ Medulloblastoma

Roselia Ciccone[1], Concetta Quintarelli[1,2], Antonio Camera[1], Michele Pezzella[1], Simona Caruso[1], Simona Manni[1], Alessio Ottaviani[1], Marika Guercio[1], Francesca Del Bufalo[1], Maria Cecilia Quadraccia[1], Domenico Orlando[1], Stefano Di Cecca[1], Matilde Sinibaldi[1], Mariasole Aurigemma[1], Laura Iaffaldano[1], Andrea Sarcinelli[1], Maria Luisa D'Amore[1], Manuela Ceccarelli[1], Francesca Nazio[1], Veronica Marabitti[1], Ezio Giorda[3], Marco Pezzullo[3], Cristiano De Stefanis[3], Andrea Carai[4], Sabrina Rossi[5], Rita Alaggio[5], Giada Del Baldo[1], Marco Becilli[1], Angela Mastronuzzi[1], Biagio De Angelis[1], and Franco Locatelli[1,6]

ABSTRACT

Purpose: Medulloblastoma (MB), the most common childhood malignant brain tumor, has a poor prognosis in about 30% of patients. The current standard of care, which includes surgery, radiation, and chemotherapy, is often responsible for cognitive, neurologic, and endocrine side effects. We investigated whether chimeric antigen receptor (CAR) T cells directed toward the disialoganglioside GD2 can represent a potentially more effective treatment with reduced long-term side effects.

Experimental Design: GD2 expression was evaluated on primary tumor biopsies of MB children by flow cytometry. GD2 expression in MB cells was also evaluated in response to an EZH2 inhibitor (tazemetostat). In *in vitro* and *in vivo* models, GD2+ MB cells were targeted by a CAR-GD2.CD28.4-1BBζ (CAR.GD2)-T construct, including the suicide gene inducible caspase-9.

Results: GD2 was expressed in 82.68% of MB tumors. The SHH and G3–G4 subtypes expressed the highest levels of GD2, whereas the WNT subtype expressed the lowest. In *in vitro* coculture assays, CAR.GD2 T cells were able to kill GD2+ MB cells. Pretreatment with tazemetostat upregulated GD2 expression, sensitizing GD2dimMB cells to CAR.GD2 T cells cytotoxic activity. In orthotopic mouse models of MB, intravenously injected CAR.GD2 T cells significantly controlled tumor growth, prolonging the overall survival of treated mice. Moreover, the dimerizing drug AP1903 was able to cross the murine blood–brain barrier and to eliminate both blood-circulating and tumor-infiltrating CAR.GD2 T cells.

Conclusions: Our experimental data indicate the potential efficacy of CAR.GD2 T-cell therapy. A phase I/II clinical trial is ongoing in our center (NCT05298995) to evaluate the safety and therapeutic efficacy of CAR.GD2 therapy in high-risk MB patients.

Introduction

Medulloblastoma (MB) is the most common malignant embryonal brain tumor of childhood, accounting for about 20% of all pediatric central nervous system malignancies. The World Health Organization (WHO) has classified MB as a grade 4 tumor that originates from neuronal precursors located in the posterior cranial fossa (1, 2). Histologically, MB is classified into four variants: classic, large cell/anaplastic (LCA), with extensive nodularity (MBEN), and desmoplastic/nodular (DN; refs. 1, 3, 4). Molecularly, MB has been reclassified into four main molecular subgroups according to the altered cellular pathway or genomic variations harbored, namely, sonic hedgehog-activated (SHH), group 3 (G3), group 4 (G4), and wingless-activated (WNT) MB. Nowadays, the mainstay of MB treatment is based on a combination of surgical resection of the tumor, craniospinal irradiation (for children ≥ 3 years of age), and adjuvant chemotherapy (5–7). Despite this intensive approach, about 30% of patients have a fatal outcome because of relapsed/resistant disease (8, 9). Furthermore, long-term survivors often experience side effects that dramatically affect their quality of life. Patients belonging to distinct MB subgroups show different outcomes, although receiving the same therapies (4). In particular, the WNT subgroup has a very good prognosis compared with other MB subgroups (5-year survival rate of 90%; refs. 1, 10), whereas the G3 subgroup is associated with the worst prognosis, presenting an overall survival (OS) rate of about 50% (1).

Chimeric antigen receptor (CAR) T-cell immunotherapy represents an innovative approach that has already shown impressive results in patients with B-cell lymphoid malignancies (11), thus giving hope to patients with other tumors. In particular, in the past few years, the immunotherapy based on the transfer of T cells engineered to express anti-GD2 CARs (GD2.CAR) to target tumor cells has emerged as an exciting new approach for several solid cancers, including neuroblastoma (12), H3K27M-mutated diffuse midline gliomas (13, 14), and lung cancers (15).

GD2 is a disialoganglioside highly expressed by neuroblastoma, melanoma, retinoblastoma, many Ewing sarcomas, osteosarcoma, soft-tissue sarcoma, small cell lung cancer, and glioma cells, with

[1]Department of Onco-Haematology and Cell and Gene Therapy, Bambino Gesù Children's Hospital, IRCCS, Rome, Italy. [2]Department of Clinical Medicine and Surgery, Federico II University of Naples, Naples, Italy. [3]Research Laboratories, Bambino Gesù Children's Hospital, IRCCS, Rome, Italy. [4]Neurosurgery Unit, Department of Neuroscience and Neurorehabilitation, Bambino Gesù Children's Hospital, IRCCS, Rome, Italy. [5]Department of Laboratories, Pathology Unit, Bambino Gesù Children's Hospital, IRCCS, Rome, Italy. [6]Department of Life Sciences and Public Health, Catholic University of the Sacred Heart, Rome, Italy.

R. Ciccone, C. Quintarelli, and A. Camera share first authorship of this article.

B. De Angelis and F. Locatelli share last authorship of this article.

Corresponding Authors: Biagio De Angelis, San Paolo N°15 Street, 00146 Rome, Italy. E-mail: biagio.deangelis@opbg.net; and Franco Locatelli, S. Onofrio square, 00165 Rome, Italy. E-mail: franco.locatelli@opbg.net

Translational Relevance

Medulloblastoma (MB), the most common childhood malignant brain tumor, has a fatal outcome in about 30% of patients. GD2 expression is not yet well characterized in MB patients. The CAR.GD2 T therapy has emerged as a promising new approach for GD2$^+$ solid cancers (e.g., neuroblastoma). GD2 was found overexpressed in the SHH and G3/G4 subgroups of MB at diagnosis, and found to be regulated in this setting by the EZH2 inhibitor tazemetostat. CAR.GD2 T cells have shown remarkable efficacy and safety profiles in both *in vitro* and *in vivo* models of MB. The dimerizing drug AP1903 was able to cross the blood–brain barrier and activate the suicide gene inducible caspase-9 (iC9) safety switch with prompt elimination of both blood-circulating CAR.GD2 T cells and those infiltrating the animal brain tumor. Our experimental data support the feasibility of a phase I/II clinical trial for a CAR.GD2 T-cell adoptive therapy approach for GD2$^+$ MB patients.

limited expression in normal tissues (16). Moreover, it has been reported that GD2 is involved in tumor development, mediating an increase of cell proliferation, growth, motility, migration, adhesion, and invasion, in small cell lung cancers (17) and breast cancer (18). In addition, it exerts an immunosuppressive activity through the interaction with the inhibitory immunoreceptor Siglec-7 (19). Recently, Paret and colleagues reported a GD2 expression study in a restricted number of patients with MB (20–22). There is therefore a need to broaden the evaluation of this antigen on a wider cohort of patients. In this study, we investigated in preclinical models the feasibility of adoptive immunotherapy using GD2 as a target for treating MB patients using a third-generation CAR construct that includes CD28 and 4.1BB as costimulatory domains (CAR.GD2 T cells), recently validated in both neuroblastoma (12, 23, 24) and high-grade glioma models (25). We tested its safety and efficacy in children with relapsed/refractory neuroblastoma (NCT03373097). Preclinical and clinical data show that the heterogeneity of target antigen expression on tumor cells may reduce the therapeutic efficacy of a CAR T-cell gene therapy (26).

Low-GD2-expressing tumor cells demonstrated significantly reduced expression of the ganglioside synthesis enzyme ST8SIA1 (GD3 synthase; refs. 27, 28). Enhancer of zeste homolog 2 (EZH2) is a histone-lysine N-methyltransferase of histone 3 (H3K27; refs. 29, 30), which facilitates chromatin compaction and represses the genes involved in GD2 biosynthesis such as the GD3 synthase (27, 31). Inhibition of EZH2 with the US Food and Drug Administration (FDA)–approved drug tazemetostat reestablishing expression of sialyltransferase GD3 synthase (GD3S; ST8SIA1) could restore the GD2 expression on tumor cells. In light of this observation to overcome the limitation of low GD2 expression on cancer cells derived from extracranic tumors, several authors considered the use of the epigenetic drug tazemetostat, to increase the antigen expression on tumor cells (15, 27, 31). We sought to evaluate whether the inhibition of EZH2 could be effective in upregulating GD2 expression also in MB cells.

Although the GD2 expression on healthy tissues has been anecdotal so far, and the lack of significant expression of this target antigen on healthy tissues has been largely proved by several trials applying the use of CAR.GD2 T cells in which no specific neurotoxicity has been reported (14, 32, 33), researchers are largely aware of the peculiar toxicity that could be associated with the use of CAR T cells in central nervous system (CNS) tumors (14, 34–36). Thus, we included in our

CAR construct an inducible caspase 9 (iC9), as a safety switch. The iC9 is a suicide gene able to be activated through binding with a synthetic small-molecule drug commonly used as a chemical inducer of dimerization, known as AP1903. Indeed, AP1903 is able to activate the dimerization domain of iC9 molecule and promote a rapid induction of apoptosis in activated CAR T cells (12, 37).

Thus, we also evaluated the efficacy of iC9 suicide gene activation to eliminate circulating and tumor-infiltrating CAR.GD2 T cells, infused into an orthotopic MB mouse model.

Materials and Methods

Peripheral blood and tumor tissues from MB patients

Tumor tissues were collected from a cohort of 52 pediatric patients with MB, classified according to WHO 2021 classification (38), at the Bambino Gesù Children's Hospital (OPBG), Rome, Italy. Patient tissues and blood samples of both patient and healthy donors were collected and evaluated by cytofluorimetric analysis for GD2 expression. All patients' legal guardians provided written informed consent and the whole research was conducted under institutional review board–approved protocols in accordance with the Declaration of Helsinki (Ethical Committee Approvals Protocol GD2CAR02 N°1203).

Cell lines and PDX

The D283 Med (G3/G4 subgroup) and DAOY (SHH subgroup; ref. 39) MB cell lines were obtained from the American Type Culture Collection (ATCC). Med 411-FHTC (G3 subgroup) and Med-411 FH mCherry/Luciferase (Med-411 FH mCherry/Luc) were purchased from Brain Tumor Resource Laboratory of Fred Hutchinson Cancer Research ("FHCRC"). DAOY and D283 Med cells were cultured according to the supplier recommendations (ATCC). Med 411-FHTC were cultured in NeuroCult NS-A Basal Medium supplemented with 50 mL of NeuroCult Supplement (STEMCELL Technologies), epidermal growth factor (20 ng/mL), fibroblast growth factor (10 ng/mL), and 1% penicillin–streptomycin for a minimum of 48 hours before experiments. Primary human lung fibroblasts (ATCC PCS-201-013) is a primary cell line obtained from normal human lung tissue. Lung fibroblasts were cultured according to the supplier recommendations (ATCC). They were cultured in basal medium (ATCC PCS-201-030) supplemented with Fibroblast Growth Kit–Low serum (ATCC PCS-201-041), composed of L-glutamine 7.5 mmol/L, rh FGF basic 5 ng/mL, ascorbic acid 50 μg/mL, hydrocortisone hemisuccinate 1 μg/mL, rH insulin 5 μg/mL, FBS 2%. Human Schwann cells (AcceGen) were cultured in Schwann cell basal medium and Schwann cell growth supplement 500× (AcceGen) supplemented with FBS. Cells were maintained in a humidified atmosphere containing 5% CO_2 at 37°C and were routinely tested for mycoplasma and for surface expression of target antigens. All cell lines have been authenticated by STR analysis in the certificated lab "BMR Genomics s.r.l."

Retroviral vectors

A retroviral vector carrying a third-generation iC9 suicide gene (as safety switch) in frame with CAR-GD2.CD28.4-1BBζ (CAR.GD2), characterized by the anti-GD2 single chain variable fragment (scFv) 14.G2a and two costimulatory domains CD28.4-1BB fused to the CD3-ζ chain, was used to transduce T cells, as previously reported (12). An additional retroviral vector carrying an eGFP-Firefly-Luciferase (eGFP-FFLuc) was used to genetically modify the D283 Med and DAOY MB cell lines in D283 Med-GFP-FF-Luc (D283 Med) and DAOY-GFP-FF-Luc (DAOY), respectively, for *in vitro* and/or *in vivo*

studies. Viral supernatant was produced by the use of the producer cell line 293VEC-RD114 (kindly provided by BioVec Pharma).

Generation of CAR T cells

Peripheral blood mononuclear cells (PBMC) were isolated from buffy coats obtained from healthy donors (HD; OPBG Hospital, Rome, Italy) who signed a written informed consent, in accordance with rules set by the Institutional Review Board of OPBG (Approval of Ethical Committee N969/2015 prot. N 669LB). T lymphocytes were activated with OKT3 (1 mg/mL, e-Bioscience Inc) and anti-CD28 (1 mg/mL, BD Biosciences) monoclonal antibody (mAb) in the presence of recombinant human interleukin-7 (IL7, 10 ng/mL; R&D Systems) and interleukin-15 (IL15, 5 ng/mL; R&D Systems). Activated T cells were transduced with CAR-GD2.CD28.4-1BBζ retroviral supernatant on day 3 as previously described (12) to obtain CAR.GD2 T cells, which were expanded in culture medium containing 45% RPMI-1640, 45% Click's medium (Sigma-Aldrich, Co.), supplemented with 10% inactivated-FBS North (Gibco, Thermo Fischer), and 2 mmol/L GlutaMax (Thermo Fischer) and replenished twice a week.

Immunophenotype analysis

Cell-surface expression of GD2 was analyzed on tumor fresh biopsies and peripheral blood (PB) of MB patients using conjugated mouse anti-human GD2-BV421 mAb (Clone 14.G2a, BD Biosciences). Intratumoral biopsies were obtained during image-guided surgery for tumor debulking, to avoid collecting normal tissues. The absence of nonpathologic cells in the tumor specimens analyzed for GD2 expression was confirmed by pathologists.

Cells were stained with live/dead dye, namely, 7-Amino-Actinomycin D (7-AAD) staining solution (BD Biosciences), CD45 APC (BD Biosciences), and the GD2 expression was evaluated on the CD45 negative (CD45$^-$) singlet cell gate.

The expression of CAR.GD2 on T cells was assessed using a specific primary anti-idiotype antibody (1A7; ref. 40), followed by a Rat Anti-Mouse Kappa PE (BD), and was evaluated in association with CD3-specific mAb.

Treated mice underwent periodical blood collection for fluorescence-activated cell sorting (FACS) analysis. PB of mice, after lysis of red blood cells with lysis buffer (BD), was stained with anti-human CD45 BUV805 (BD Biosciences), anti-human CD3 Pecy7 (BD Biosciences), anti-human CD4 BUV605, anti-human CD8 BUV395 (BD Biosciences) in combination with 1A7-PE anti-idiotype antibody. Cells were incubated with mAbs (30 minutes at 4°C in the darkness), then washed in 1× phosphate-buffered saline (1× PBS) and acquired with a FACS-Fortessa flow-cytometer. Data were analyzed by FACS-Diva software (BD FACSDiva Software, RRID:SCR_001456; Becton Dickinson). For each sample, we analyzed a minimum of 20,000 events.

Coculture assay

For *in vitro* coculture assay, the untransduced effector (E) T cells (NT-T) or CAR.GD2 T cells (0.1 × 10^6 cells/well) were plated with the GD2$^+$ target (T) MB cells in a 24-well plate at the indicated effector: target (E:T) ratio for 5 days. The antitumor effect was evaluated by flow-cytometry assay, assessing the percentage of residual live 7AAD^{negative} GD2^{positive} (7AAD$^-$GD2$^+$) tumor cells or absolute quantization of GD2$^+$ tumor cells remaining in culture after exposure to NT-T or CAR.GD2 T cells. CountBright absolute counting beads (Thermo Fisher Scientific) were used for the absolute quantification of tumor cells.

IncuCyte live-cell analysis

CAR.GD2 T-cell cytotoxicity activity was also tested by using the IncuCyte S3 live-cell imaging system (Sartorius). GFP$^+$ tumor cells were seeded in a 24-well plate. After tumor cells adhered to the plates, T cells were added into each well at a final volume of 2 mL per well with E:T ratios of 1:1. A three-dimensional (3D) culture with the DAOY cell line was performed in a 96 Ultra Low Attach multiwell plate to investigate GD2 expression based on cell density. The growth of spheroids was daily monitored up to a diameter of 300 µm by IncuCyte Live-Cell imaging. At 72 hours of culture, spheroids were collected and analyzed by FACS for GD2 expression level.

The IncuCyte Live-Cell Analysis System was applied as a real-time quantitative live-cell imaging and analysis platform that enables the visualization and quantification of cell behavior over time, by automatically gathering and analyzing images around the clock within a standard laboratory incubator. The Total Green Object Integrated Intensity or Green Area Confluence parameter was chosen to visualize and quantify tumor cells' behavior over time.

Cytokine profile

Supernatants were collected after 24 hours of coculture of tumor cells and CAR.GD2 T cells to evaluate cytokine release. Cytokines were measured by immunoassay in a microfluidic Simple Plex cartridge ELLA (Biotechne; R&D Systems). In particular, we investigated the following molecules and cytokines: granzyme B, interferon-gamma (IFNγ), IL2, and tumor necrosis factor alpha (TNFα). Moreover, the murine plasma levels of circulating neurofilament light chain (NFL; Biotechne; R&D Systems) have been quantified as a marker of neuronal damage injury (41).

Xenograft MB mouse model for *in vivo* studies

NOD/SCID IL2Rγnull (NSG) xenograft mice were purchased from Charles River and maintained in the Plaisant Castel Romano animal facility in Rome. Mice experiments were conducted in compliance with the EU and national ethical requirements and were approved by the Italian Health Ministry (n° 765/2021-PR). For the orthotopic *in vivo* model, 5-week-old female and/or male NSG mice were anesthetized by intraperitoneal injection of ketamine (10 mg/kg) and xylazine (100 mg/kg). The posterior cranial region was shaved and placed in a stereotaxic head frame. Tumor cell lines were evaluated by FACS for GD2 expression before the infusion. D283 MED cells (2 × 10^5/each mouse) were stereotaxically implanted into the cerebellum at an infusion rate of 1 µL/minute by using the following coordinates, according to the atlas of Franklin and Paxinos: 6.6 mm posterior to the bregma; 1 mm lateral to the midline; and 2 mm ventral from the surface of the skull. After injection, the cannula was kept in place for about 3 minutes for equilibration of pressures within the cranial vault. The skin was closed over the cranioplastic assembly using metallic clips. After 3 days of tumor engraftment, mice were randomly divided into two groups, injected intravenously (i.v.) with either 10×10^6 control NT T cells or CAR.GD2 T cells of 2 different donors (HDs), and subjected to weekly bioluminescence imaging (IVIS Spectrum *in vivo* imaging system, PerkinElmer) until the end of the experiment (day 90). Signal quantitation of photons/second/cm^2/stereoradiant (p/sec/cm^2/sr) was performed as previously described (42, 43). Moreover, we established an MB patient-derived xenograft (PDX-MB) mouse model by stereotaxic implantation of Med-411FH mCherry-/Luciferase cells (2 × 10^5/each mouse). Fourteen days following tumor implantation, mice received i.v. either NT T cells or CAR.GD2 T cells (10 × 10^6/each mouse) and were monitored for tumor growth by IVIS imaging until 60 days (end of the experiment).

Two stereotaxic models of DAOY (2×10^5/each mouse) were developed to evaluate the antitumor efficacy of CAR.GD2 T cells. In the first experiment, we implanted DAOY tumor cells for 10 days before T-cell infusion. Mice were then randomly divided into two groups and injected intravenously (i.v.) with 10×10^6 control NT T cells or CAR.GD2 T cells. Tumor growth was weekly monitored by IVIS imaging until day 90 (end of the experiment). In the second experiment, we implanted DAOY tumor and at day +3 mice were randomly divided into two groups: untreated (16 mice) and treated cohort with Tazemetostat (S7128-21GR, Selleck Chemicals; 16 mice) that received 400 mg/kg oral gavage, bis in die (b.i.d.) for 10 days, formulated according to the protocol previously reported (44). At day +14, 3 mice of each group were sacrificed and brain tumors were analyzed by FACS to evaluate the GD2 expression. At day +15, mice were randomly divided into six groups: untreated or i.v. treated with NT or CAR.GD2 T cells (10×10^6/each mouse). Tumor growth was weekly monitored by IVIS imaging.

All mice were sacrificed according to protocol when moribund or upon the development of hind-limb paralysis. In all above-mentioned *in vivo* experiments, the mice weight (grams) was monitored daily and the expansion of effector cells was monitored every 2 weeks by blood bleedings and analyzed by flow cytometry using BD LSRFortessa X-20. Data were analyzed using the FACSDiva software or FlowJo Software (BD Biosciences).

In vitro and *in vivo* study of the activation of the suicide gene by dimerizing drug AP1903 infusion

For *in vitro* experiments, CAR.GD2 T and or NT T cells were exposed to 10 nmol/L AP1903 (cat. no. 6130, Biotechne-tocris.) for 24 hours and residual viable cells were stained with Annexin-V/7AAD (BD Pharmingen) and analyzed by FACS analysis.

The *in vivo* activity of AP1903 to induce apoptosis of CAR.GD2 T cells was assessed in *in vivo* PDX (Med411 FH mCherry/Luciferase) MB mouse model. Briefly, 2×10^5 tumor cells were orthotopically infused in 5-week-old NSG mice. After tumor engraftment, confirmed by bioluminescence monitoring, mice received an intravenous injection (i.v.) of 10×10^6 of NT T or CAR.GD2 T cells. Level of circulating CAR.GD2 T cells was monitored by FACS analysis and when the level of CAR.GD2 T cells in PB was ≥ 35% (Med411 FH mCherry/Luciferase), mice received three consecutive doses (on day +11, day +12, and day +13 after T-cell infusion) of either placebo or AP1903 (100 μg/day/mouse, cat. no. 6130, Biotechne-tocris) by intraperitoneal (i.p.) infusion. The residual effector T cells were evaluated 24 hours after the last AP1903 treatment by flow cytometry in the PB and through IHC analysis in brain/tumor tissues. Animals were sacrificed and brains were fixed in 4% formaldehyde in 0.1 mol/L phosphate buffer (pH 7.2) and paraffin embedded.

Hematoxylin/eosin and immunohistopathological analysis on mouse tissues

The histopathologic analysis was performed as previously reported (43). Briefly, after hematoxylin/eosin staining for IHC analysis, the sections were cut to 2.5 μm thick, dewaxed, and rehydrated. Epitope retrieval was performed by boiling the slides with EDTA (pH 9). Endogenous peroxidase was blocked with 3% hydrogen peroxide for 10 minutes, followed by another blocking step in 5% serum albumin (BSA) for 1-hour RT. The sections were then incubated with anti-CD3 antibody (1:100, Dako) or anti-Ki67 (1:100, Abcam) at 4°C overnight. The secondary biotinylated antibody (K8024, Dako) and the peroxidase DAB kit (Dako) were used to reveal the primary antibodies. Slides were then counter-stained with hematoxylin, dehydrated with a series of alcohol solutions (70%–100%), followed by three changes of Diasolv, and mounted with Diamount (Diapath). Analysis was performed using standard microscopy.

Treatment of tumor cells with enhancer of zeste homolog 2 inhibitor

The MB cell lines (DAOY, MED-411 FHTC) were seeded in 6-well plates at 1×10^5 cells/well. Tumor cells were treated with the EZH2 inhibitor tazemetostat (S7128-10MM, Selleck Chemicals) dissolved in dimethyl sulfoxide (DMSO) at a concentration of 1 or 10 μmol/L or DMSO alone. Cells were incubated at 37°C and 5% CO_2 for 7 days. When the medium was changed or cells were split, the EZH2 inhibitor was replenished at the same concentration. At day 7 of treatment, cells were harvested and analyzed for the GD2 expression by flow cytometry and used for functional studies.

Statistical analysis

Data are presented as mean ± SD or mean ± SEM. Student *t* test or ordinary two-sided/one-way ANOVA (Bonferroni/Tukey multiple comparisons test) was used, where appropriate, for comparing differences between groups. The Kaplan–Meier method was used to estimate OS probabilities and disease-free survival (DFS) probabilities, with disease being defined by bioluminescence higher than 10E8 p/sec/cm^2/sr and/or appearance of the sign of sufferance. Differences between groups were compared with the log-rank test. Mice were matched based on the tumor signal for control and treated groups. Graph generation and statistical analyses were performed using Prism version 10.1.0 software (GraphPad Prism, RRID:SCR_002798). Wilcoxon, Mann–Whitney nonparametric or log-rank tests were used. In all cases, a $P \leq 0.05$ was considered statistically significant and reported as follows: *, $P < 0.05$; **, $P \leq 0.01$; ***, $P \leq 0.001$; ****, $P \leq 0.0001$.

Ethics approval and consent to participate

Written informed consent was obtained from each donor. The studies were approved by the Institutional Ethical Committee GD2CAR02 No. 1203. Mouse experiments were conducted in compliance with the international, EU, and national ethical requirements and were approved by the Italian Health Ministry (No. 765/2021-PR).

Data availability statement

All data associated with this study are presented in the paper and supplementary data (i.e., videos). Raw data generated in this study are available upon reasonable request from the corresponding authors, upon an agreement signed between the parties for their specific use.

Results

GD2 expression in primary MB biopsies and MB cell models

To investigate whether MB could be a suitable target for CAR.GD2 T cells, we evaluated GD2 expression on fresh specimens of tumor biopsies of 52 MB patients treated at our institution (**Fig. 1**; Supplementary Fig. S1). The flow-cytometry analysis performed on tumor tissues showed a positive, although heterogeneous, expression of GD2 in 82.68% of the analyzed samples, with an average of 50.46 ± 35.90% GD2-positive cells (among CD45$^-$ cells). The presence of nontumoral cells in the tumor biopsy was considered negligible by the pathologist. PBMCs of the same MB patients were analyzed in parallel, as internal negative control of GD2-positive cells, being equal to 0.24 ± 0.28% ($P < 0.0001$; **Fig. 1A**). The median fluorescence intensity (MFI) for GD2 expression was significantly higher on MB tissue biopsies
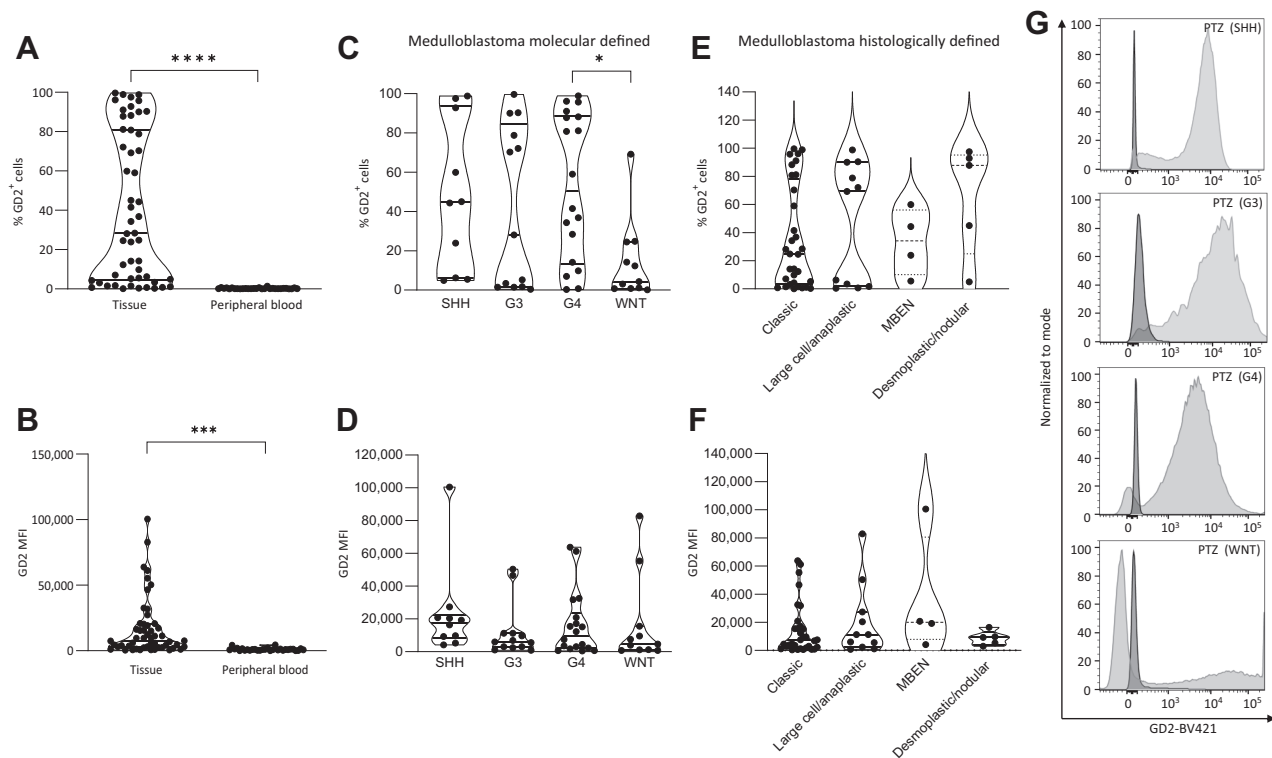
Figure 1.
GD2 is highly expressed in tumor tissues from pediatric MB patients. **A,** The percentage of GD2 expression levels on cells of tumor biopsies and PB obtained from pediatric MB patients at diagnosis were assessed by flow-cytometry analyses. **B,** MFI for GD2 on cells obtained from tumor biopsies and PB of pediatric MB patients at diagnosis. **C** and **D,** The percentage of GD2-positive cells (**C**) and GD2 MFI (**D**) in MB samples stratified according to the molecular subgroups (SHH, G3, G4, and WNT subgroups). **E** and **F,** The percentage of GD2-positive cells (**E**) and GD2 MFI (**F**) in MB patients stratified by the histologic classification [classic, large cell/anaplastic (LCA), with extensive nodularity (MBEN) and desmoplastic/nodular (DN) subgroups]. The violin plots of the GD2$^+$ cells (**A, C,** and **E**) or GD2 MFI (**B, D,** and **F**) are shown as the frequency distribution of the data using five summary values: the minimum, first quartile (bottom horizontal line), median, third quartile (upper horizontal line) and the maximum value. **G,** FACS plot of GD2 expression in a representative patient of SHH (I plot), G3 (II plot), G4 (III plot), and WNT (IV plot) subgroups. Isotype control is shown in dark gray. *, $P < 0.05$; **, $P < 0.01$; ***, $P \leq 0.001$; ****, $P \leq 0.0001$.

(17,176.9 ± 22,406.4) than on cells from PB samples (1,067.5 ± 1,042.5, $P < 0.0001$; **Fig. 1B**). Interestingly, when we stratified MB samples according to the molecular subgroups, we found GD2 positivity in 100% (10/10) of SHH patients (GD2$^+$: 47.88 ± 38.28%), in 88.9% (16/18) of G4 patients (GD2$^+$: 52.86 ± 37.29%), and in 76.92% (10/13) of G3 patients (41.76 ± 41.52%), whereas the WNT subgroup was characterized by a lower rate of GD2 positivity (63.64%, 7/11) and a low frequency of GD2$^+$ cells (14.09±20.5% of CD45$^-$ analyzed cells; **Fig. 1C**; Supplementary Fig. S1A–S1D). All molecular subgroups show high variability of GD2 MFI expression (**Fig. 1D**). We also stratified patients based on histologically defined subgroups, and we observed GD2 positivity in 78.13% (25/32) of patients with classic MB, 81.8% (9/11) of LCA MB, 100% (4/4) of MBEN MB and 100% of (5/5) desmoplastic/nodular (D/N) MB (**Fig. 1E** and **F**). Due to the high variability of GD2 expression (both in terms of percentage and MFI) among MB samples, the difference in GD2 positivity observed was not statistically significant among histologic subgroups (**Fig. 1E** and **F**). A representative FACS plot of GD2 expression for each molecular subgroup has been shown in **Fig. 1G**. Finally, we evaluated the expression of GD2 in four MB cell lines (Supplementary Fig. S2). In particular, the D283 Med (G3/G4 subgroup) cell line and MED-411 FH mCherry/Luciferase (G3 subgroup) showed the highest GD2 expression (GD2: 99.6% ±

0.1% in D283 and 99.1% ± 0.4% in MED-411 FH; MFI: 42,354.0 ± 2119.4 in D283 and 22,127 ± 861.3 in MED-411 FH). DAOY (SHH subgroup) cell line showed 82.4% ± 10.8% GD2$^+$ cells with an MFI of 15,589.0 ± 648.0 and the cell lines Med 411-FHTC (G3 subgroup) showed 46.1% ± 3.8% GD2$^+$ cells with a MFI of 2011.67±946.8 (Supplementary Fig. S2A–S2C). The expression of GD2 in the DAOY, although significantly lower than in the MB D283 Med cell line, is influenced by cellular confluence in both 2D and 3D models (Supplementary Fig. S2D and S2E). However, GD2 expression in the PDX Med 411-FHTC cell line, which grows as multicellular aggregates in suspension and some adherent cells, does not appear to increase significantly with increasing cell density (Supplementary Fig. S2F).

CAR.GD2 T cells exert effective antitumor activity toward human GD2$^+$ MB cell lines

Having shown a relevant expression of GD2 in most samples of MB patients, we then tested the *in vitro* cytotoxic activity of our third-generation CAR.GD2 T cells against D283 Med (G3/G4 subgroup), DAOY (SHH subgroup), and the MB-PDX cell line Med 411-FHTC (G3 subgroup).

The CAR-GD2.CD28.4-1BBζ retroviral vector (12) includes CD28 and 4-1BB, as costimulatory domains, and the iC9 suicide gene, as a

safety switch (Supplementary Fig. S3A). The transduction efficiency of CAR.GD2 T cells was equal to 82.62% ± 10.78% (Supplementary Fig. S3B and S3C).

The iC9 functionality was evaluated after 24 hours of *in vitro* treatment with AP1903, showing a significant reduction in the percentage of CAR.GD2 T cells (see Supplementary Fig. S3D).

In *in vitro* long-term coculture assays, NT T cells and CAR.GD2 T cells, derived from five different HD, were incubated for 5 days with D283 Med, DAOY, or MED 411-FHTC cells at the E:T ratio of 1:1 (**Fig. 2**).

CAR.GD2 T cells were able to significantly kill D283 Med cells compared with NT T cells (GFP-residual tumor: 1.0% ± 1.0% vs. 88.2% ± 6.3%, respectively, $P < 0.0001$; **Fig. 2A**, left), and MED 411-FHTC cells compared with NT T cells (GFP-residual tumor: 10.1% ± 6.2% vs. 51.8% ± 19.2%, respectively, $P < 0.001$; **Fig. 2C**, left). Moreover, cytokine production strongly correlated with the high anti-MB killing activity displayed by CAR.GD2 T cells (**Fig. 2D**, and **F**). Indeed, significantly higher amounts of granzyme B, IFNγ, IL2, and TNFα were produced by CAR.GD2 T cells upon coculture with GD2^{+} D283 Med (**Fig. 2D**) or MED 411-FH MB cell lines (**Fig. 2F**), as compared with control NT T cells. By contrast, when CAR.GD2 T cells were cocultured with DAOY cells, characterized by a low percentage and MFI of GD2 antigen (Supplementary Fig. S2B and S2C), we observed a suboptimal antitumor response, although statistically significant, with a higher percentage of resid-

ual tumor at the end of coculture compared with NT T cells (GFP-residual tumor: 27.88% ± 12.88% vs. 51.36% ± 13.24%, respectively, $P = 0.03$; **Fig. 2B**, left), and in parallel, by a minimal production of activating cytokines (**Fig. 2E**). To have a deeper understanding of the kinetics of CAR.GD2 T-cell killing of D283 Med and DAOY MB cell lines, a coculture monitored in real-time by an imaging system (IncuCyte) was performed. Notably, 14 hours after the beginning of coculture (Supplementary Fig. S4A), we could already observe a reduction in tumor growth in the D283 Med cell line, as evidenced by the analysis of remaining GFP^{+} tumor cells (Supplementary Fig. S4A and S4B and Supplementary Video S1A–S1C). The same kinetics of CAR.GD2 T-cell activity was also observed for DAOY coculture but with an incomplete tumor cell killing and a high percentage of residual tumor at the end of the experiment (Supplementary Fig. S5A–S5B and Supplementary Video S2A–S2C). For this reason, we investigated by flow-cytometry the residual DAOY cells, resistant to the elimination by CAR.GD2 T cells, and we observed that the spared DAOY cells were mostly GD2 negative or with very low GD2 MFI, as shown in exemplificative FACS analysis (Supplementary Fig. S6A and S6B).

Inhibition of EZH2 in GD2^{low} MB cell lines increases GD2 expression in *vitro* MB cell lines

Recently, the EZH2 inhibitor tazemetostat has been reported to effectively increase cell-surface expression of GD2 on Ewing
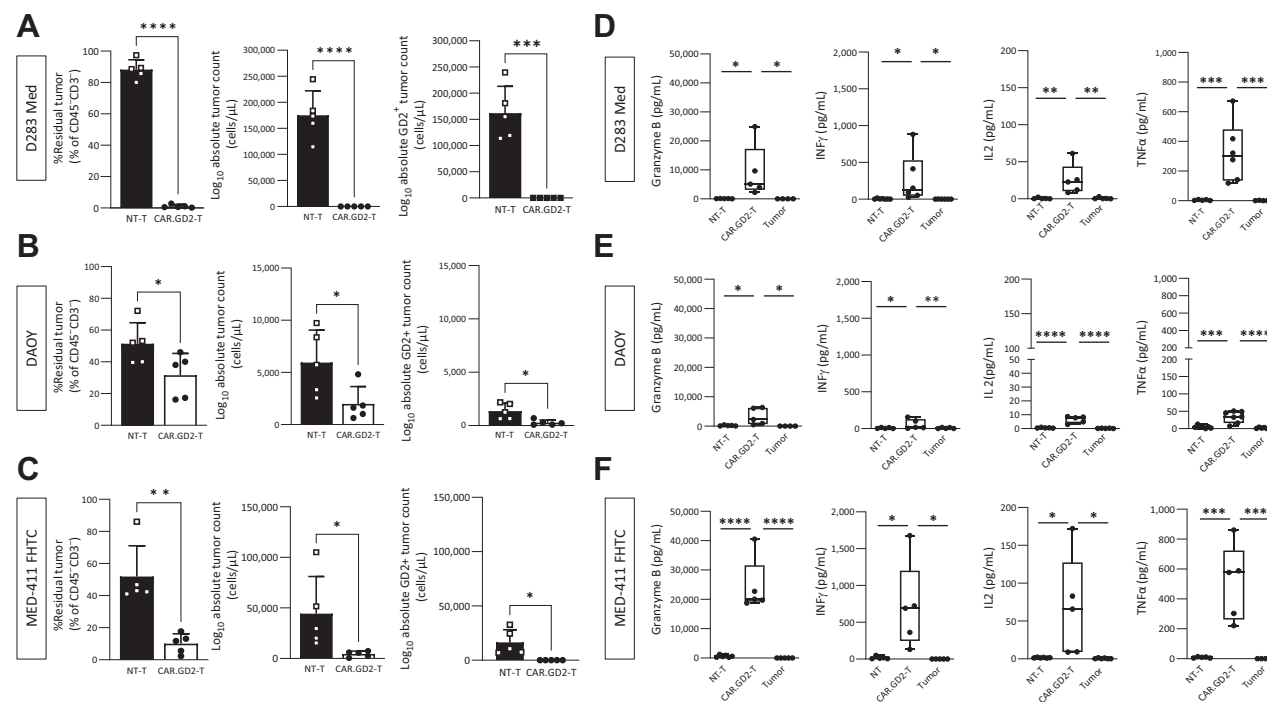

Figure 2.

In vitro antitumor activity of CAR.GD2 T cells against human GD2^{+} MB cell lines and MB-PDX cells. Five-day cocultures were performed in five independent experiments, in which GD2^{+} MB cell lines D283 Med (**A**), DAOY (**B**), and the PDX MED-411 FH (**C**) were cocultured with either NT-T (white square symbol) or CAR.GD2 T cells (black circular symbol), derived from 5 different HDs, at the E:T ratio of 1:1. The residual tumor, defined as CD45-negative CD3-negative (CD45⁻CD3⁻) tumor cells, is expressed as percentage (left graph), total absolute count (cells/μL; middle graph), or GD2^{+} absolute count (cells/μL; right graph). Data are expressed as column bar graph showing mean ± SD. Granz B, IFNγ, IL2, and TNFα were measured by ELISA assay in the 24-hour culture supernatant of NT-T or CAR.GD2 T cells in response to GD2^{+} MB cell lines D283 Med (**D**), DAOY (**E**), or the PDX cell line MED-411 FH (**F**). Data of cytokine quantification are shown in a box and whisker plot showing the minimum value, first quartile (bottom horizontal line), median, third quartile (upper horizontal line), and the maximum value. *, $P < 0.05$; **, $P < 0.01$; ***, $P < 0.001$; ****, $P < 0.0001$.

sarcomas (31), small cell lung carcinomas, non–small cell lung carcinomas (NSCLC; ref. 15), and neuroblastoma cells (27). Given the heterogeneity of GD2 expression on MB cell lines, we investigated whether tazemetostat could also have the same effect in the context of GD2^{low} MB tumors.

DAOY (SHH) and MED-411 FHTC cell lines were cultured for 7 days with tazemetostat (1 or 10 μmol/L) or equivalent volumes of control DMSO. Tazemetostat significantly upregulates GD2 expression on both MB cell lines (**Fig. 3A–C**; Supplementary Fig. S7A–S7C), but not on key elements of the tumor microenvironment, namely, human Schwann cells, T cells, and primary normal fibroblasts (Supplementary Fig. S8A and S8B).

The upregulation of the GD2 target antigen induced by exposure to low or high concentrations of tazemetostat was mirrored by an increased elimination by CAR.GD2 T cells of treated DAOY cells, as demonstrated in 5 days long-term coculture (**Fig. 3C**). The relevance of the synergic use of tazemetostat and CAR.GD2 T cells was also assessed in a cytotoxicity functional assay performed with a real-time analysis system (IncuCyte; Supplementary Fig. S9A–S9C).

Exposing the tumor to tazemetostat for seven days did not directly influence the growth of the DAOY cell line (Supplementary Fig. S9A). However, it did significantly enhance the tumor elimination rate when pretreated tumor cells were cocultured with CAR. GD2 T cells, as opposed to NT T cells (Supplementary Fig. S9B). The increased susceptibility to CAR.GD2 T-cell killing was evident as early as eight hours into the coculture, highlighting a significant

control of tazemetostat-treated DAOY cell growth compared with control MB cells pretreated with DMSO ($P = 0.0004$; Supplementary Fig. S9C).

CAR.GD2 T cells exert antitumor activity in xenogeneic mouse models of MB

We assessed the *in vivo* CAR.GD2 T-cell antitumor activity in a first MB NSG mouse model, using orthotopically implanted D283 Med (subgroup G3/G4) cells. The MB cell line was implanted intracranially and bioluminescent imaging (BLI) was used to monitor tumor growth over time. Three days after tumor engraftment, mice were randomized to be intravenously treated with either NT T cells or CAR.GD2 T cells, derived from two different donors (**Fig. 4A** and **B**). As expected, in mice treated with NT T cells, tumor bioluminescence rapidly increased up to 3 logs in less than one month (**Fig. 4B–D**) and mice either died or were sacrificed due to morbidity. The cohort of mice receiving CAR. GD2 T cells showed a significant tumor control after day +30 (**Fig. 4B–D**) with a significant prolongation of DFS compared with the NT T cells mice group ($P = 0.0009$; **Fig. 4E**). Mice treated with CAR.GD2 T cells showed xenograft reaction signs of human T cells with three out of eight mice dying in remission (**Fig. 4F**), probably due to a graft-versus-host disease (GVHD), with rapid weight loss, blepharitis, and alopecia. Toxicity was preceded by rapid expansion of infused T cells (**Fig. 4G** and **H**). In particular, all the mice experiencing GVHD had been treated with CAR.GD2 T cells manufactured from donor #1, characterized by a high percentage of CD4$^+$ CAR$^+$ T cells. Notably, the *in vivo* antitumor efficacy of CAR.GD2 T cells correlated
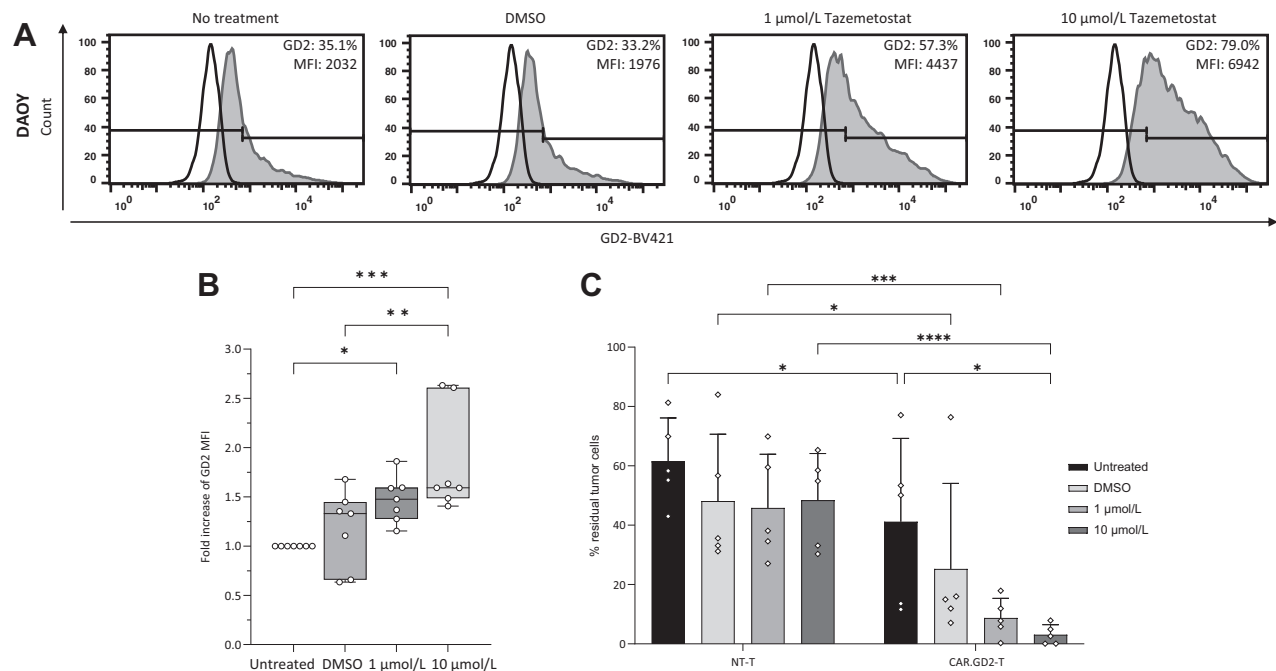

Figure 3.
Inhibition of EZH2 with tazemetostat upregulates GD2 expression in DAOY-GFP (SHH subgroup) MB cells. **A,** Representative flow-cytometry analyses of GD2 expression (percentage and MFI) in DAOY-GFP cell line treated with 1 or 10 μmol/L of tazemetostat for 7 days. DMSO vehicle was used as a negative control. **B,** Data are representative of the GD2 MFI in seven replicates of the MB DAOY-GFP cell line treated with 1 or 10 μmol/L of tazemetostat for 7 days. Values are represented with the box and whisker plot showing: the minimum value, first quartile (bottom horizontal line), median, third quartile (upper horizontal line), and maximum value. **C,** Long-term 5-day coculture of NT or GD2.CAR-28.4-1BBζ (CAR.GD2) T cells with DAOY cells (pretreated with tazemetostat or the DMSO control), at the E:T ratio of 1:1 (five different HDs). The residual tumor cells were reported as a percentage of GFP$^+$ cells. Data, average ± SD. Two-way ANOVA was used as a multicomparison test. *, $P < 0.05$; **, $P < 0.01$; ***, $P < 0.001$; ****, $P ≤ 0.0001$.
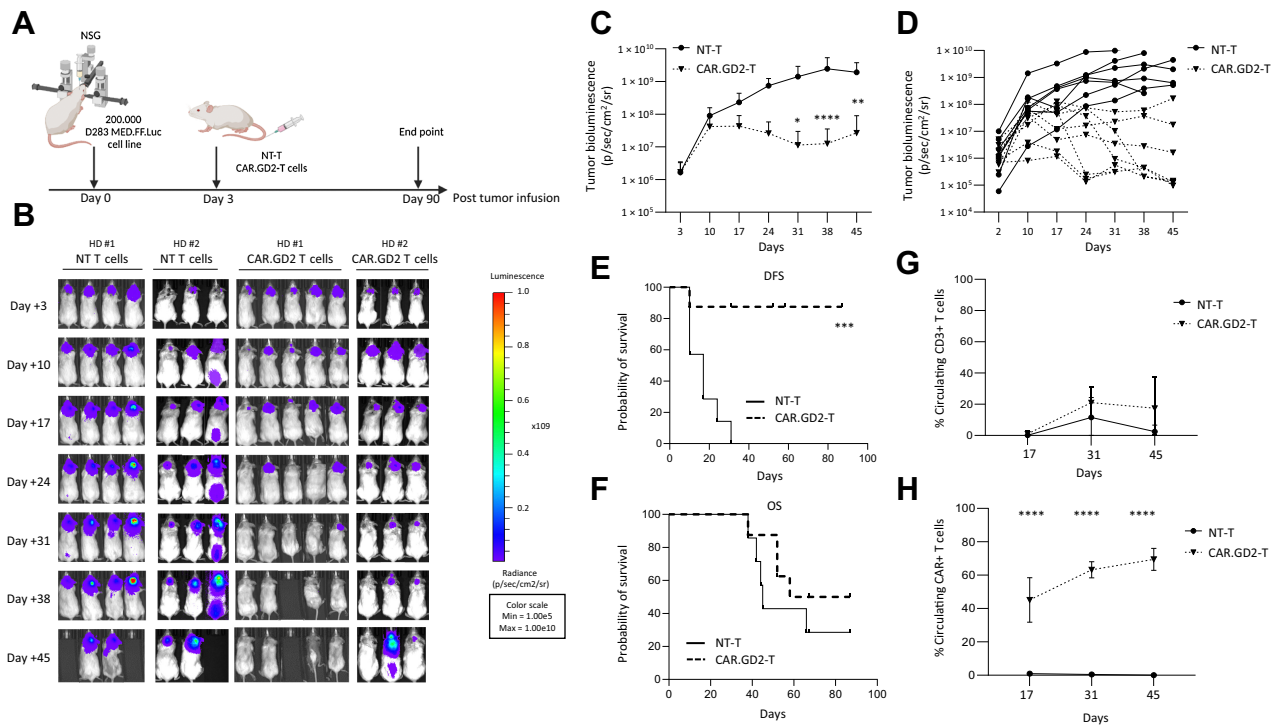
Figure 4.
Orthotopic mouse model of human D283 Med-GFP-FF-Luc cell line to evaluate antitumor activity of CAR.GD2 T cells. **A,** Illustration of the experimental design in which D283 Med-GFP-FF-Luc cell line was stereotaxically implanted into the cerebellum of 15 NSG mice. After 3 days, effector T cells derived from 2 different HDs were administered through i.v. injection. Time course of *in vivo* bioluminescence imaging of each treated NSG mouse (**B**) from day 3 (day of effector T-cell infusion). **C,** Graph shows the average of *in vivo* bioluminescence of mice treated with NT-T (continuous black line) and CAR.GD2 T cells (dotted black line). Data are shown as average ± SD derived from 2 HDs. **D,** The graph shows the bioluminescence analysis of each tumor-bearing mouse treated with NT-T (black lines with circle) or CAR.GD2-T cells (dotted black lines with triangles). **E,** Disease-free survival (DFS) of seven tumor-bearing NSG mice treated with NT T (continuous black line) or eight infused with CAR.GD2 T cells (dotted black line). **F,** Overall survival (OS) of seven tumor-bearing NSG mice treated with NT T (continuous black line) and eight tumor-bearing NSG mice infused with CAR.GD2 T cells (dotted black line). **G** and **H,** Average of circulating human T cells evaluated as % of CD45$^+$CD3$^+$ cells (**G**) and CD3$^+$CAR$^+$ cells (**H**) in NSG mice treated with NT T cells (red line) or CAR.GD2-T cells (dotted black line) at days 15, 30, and 45 after effector T-cell infusion. Data are shown as the average ± SD of 2 healthy donors (HDs). Two-way ANOVA was used as a multicomparison test. *, $P < 0.05$; **, $P < 0.01$; ***, $P < 0.001$; ****, $P < 0.0001$. (**A,** Created with BioRender.com.)

with a long-term persistence (up to day +45) of circulating effector T cells (CD45$^+$/CD3$^+$) in PB (**Fig. 4G**). More importantly, the percentage of circulating CAR$^+$ T cells remained detectable and increased over time up to day +45 (**Fig. 4H**), with a defined distribution of CD4$^+$ and CD8$^+$ T cells (Supplementary Fig. S10A and S10B).

The cytotoxic activity of CAR.GD2 T cells was also evaluated on a second orthotopic model of MB using DAOY cell line (subgroup SHH). Ten days after tumor engraftment, mice were intravenously treated with NT T cells or CAR.GD2 T cells (day 0; **Fig. 5A**). Tumor bioluminescence rapidly increased up to 2 logs in NT T cells treated mice in about 60 days after tumor cell infusion and mice either died or were sacrificed due to morbidity (**Fig. 5B** and **C**). Of the cohort of mice receiving CAR.GD2 T cells, 80% showed a complete tumor eradication by day +28 (**Fig. 5B** and **C**), translating into a significant prolongation of OS (**Fig. 5D**). After day +42, we observed a significant expansion of circulating T cells in all mice treated with CAR.GD2 T cells (46.5% ± 23.8%) compared with NT T cells (2.8% ± 5.5%, $P = 0.0039$; **Fig. 5E**). The percentage of circulating CAR$^+$ T cells remained stable for 51 days (**Fig. 5F**), until tumor eradication, and then drastically reduced in the following weeks (**Fig. 5F**). During the experiment, we noticed a significant loss of weights only in the NT T-cell mice group and

mouse #4 of CAR.GD2 T cells mice group that failed to reach a complete tumor control (**Fig. 5G**). Notable, in two mice (mouse #2 and mouse #3), treated with CAR.GD2 T cells, we observed, at day +51, a rapid expansion of circulating T cells up to 76.3% (**Fig. 5E–H**). To demonstrate that the T-cell-mediated GVHD could be controlled by direct elimination of CAR T cells, we treated mouse #2 with AP1903 (for 3 consecutive days), reaching a significant elimination of circulating CAR T cells (decreasing from 76.3% to 9.4% after AP1903 administration; **Fig. 5H**) and allowing the mouse to survive throughout the duration of the experiment. By contrast, mouse #3, without subsequent treatment, died very early. To verify whether CAR.GD2 T cells exert a peculiar neurotoxicity in this MB model, we measured the levels of murine NFL in the circulating blood. NFLs are a sensitive marker of neuroaxonal injury; their increase is also associated with neural damage induced by brain tumor/metastasis or neurotoxicity after CAR T-cell treatment (45). In our DAOY xenograft mouse model, we observed a significantly higher level of murine NFL only in mice bearing tumor alone or receiving NT T-cell mice groups (Supplementary Fig. S11). No significant increase in the NFL level was observed in CAR.GD2 T-cell–treated mice, even in mice #2 and #3 that showed a strong expansion of CAR T cells and/or alopecia.
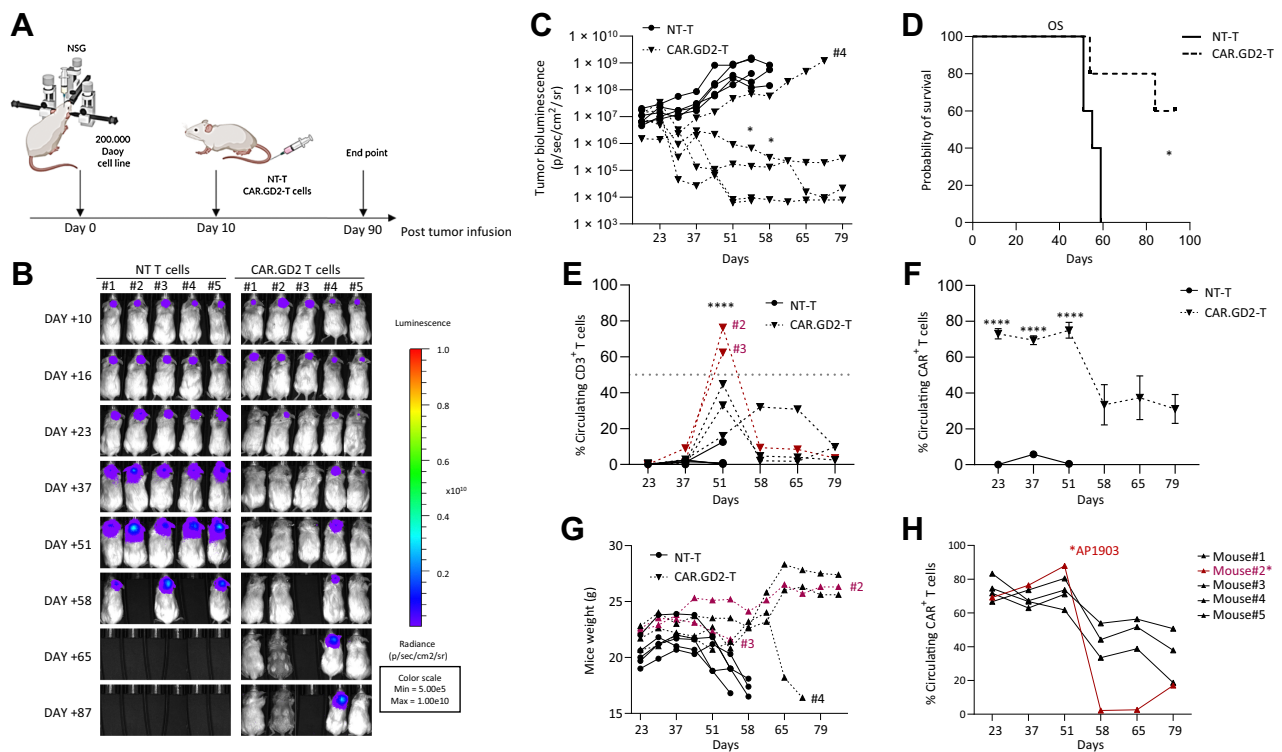
Figure 5.
Orthotopic mouse model of human DAOY-GFP cell line to evaluate antitumor activity of CAR.GD2 T cells. **A,** Illustration of the experimental design of DAOY-GFP cells stereotaxically implanted into the cerebellum of 10 NSG mice. At the time of tumor engraftment (day 10), the effector cells were administered through i.v. injection. **B,** Time course of *in vivo* bioluminescence imaging of each treated NSG mouse from day 10 (day of effector cells infusion) to day 87. **C,** The graph shows bioluminescence analysis of each tumor-bearing mouse treated with NT T cells (black lines with circle) or CAR.GD2 T cells (dotted black lines with triangle). **D,** Disease-free survival (DFS) of 10 tumor-bearing NSG mice treated with NT T cells (continuous black line) or CAR.GD2 T cells (dotted black line). Single values of circulating human T cells evaluated as % of CD45$^+$CD3$^+$ cells (**E**) and average of CD3$^+$CAR$^+$ cells (**F**) in NSG mice treated with NT T cells (black line) or CAR.GD2 T cells (dotted black line); values ≥50% of total CD3$^+$ were marked with a red curve. **G,** Values of weights (grams, g) in mice treated with NT T cells or CAR.GD2 T cells. Mouse #2 and #3 (**E** and **G**), exhibiting a strong expansion of CAR-T cells, were marked in red. **H,** Percentage of circulating CAR.GD2 T cells over time in the CAR.GD2 mice group; mouse #2 was treated with AP1903 at day 51. Data are shown as average ± SD. Two-way ANOVA was used as a multicomparison test. *, $P < 0.05$; **, $P < 0.01$; ***, $P < 0.001$; ****, $P < 0.0001$. (**A,** Created with BioRender.com.)

Pretreatment with tazemetostat enhances the antitumor activity of CAR.GD2 T cells in the MB xenograft model

We evaluated the ability of tazemetostat to cross the blood–brain barrier (BBB) and sensitize tumor cells to the cytotoxic action of CAR.GD2 T cells in an orthotopic MB model (Supplementary Fig. S12). The DAOY MB cell line was implanted intracranially in 30 NSG mice (day 0) and half of them received tazemetostat by oral gavage from day +3 to day +13 (Supplementary Fig. S12A). Bioluminescence analysis confirmed that tazemetostat treatment did not significantly affect tumor growth (Supplementary Fig. S12D).

At day +14, 3 mice of each group were sacrificed and brain tumors were analyzed by flow cytometry to assess GD2 expression. Results showed elevated GD2 expression on DAOY-explanted tissues (Supplementary Fig. S12B) and a significant increase in GD2 MFI in the tazemetostat-treated cohort compared with the untreated group (Supplementary Fig. S12C). For the remaining mice, at day +14, both tazemetostat-treated and untreated groups received intravenously NT-T cells or CAR.GD2 T cells, and tumor growth was weekly monitored by IVIS imaging (Supplementary Fig. S12D–S12F). Mice pretreated with tazemetostat and receiving CAR.GD2 T cells showed a significant early antitumor response (day +6 from T-cell infusion; Supplementary Fig. S12G). However, at day +14 from CAR.GD2 T-cell therapy, we

did not observe any difference in tumor control between the two cohorts of mice (Supplementary Fig. S12F). This finding strongly correlates with the *in vitro* evidence that tazemetostat withdrawal is associated with the reduction of the GD2 MFI level (Supplementary Fig. S13A and S13B).

Intravenously injected CAR.GD2 T cells infiltrate MB tissue, increasing the OS in PDX model of MB

To further investigate the *in vivo* functionality of CAR.GD2 T cells, a third orthotopic PDX G3 MB model was developed. In particular, NSG mice were engrafted with Med-411FH mCherry/Luciferase cells. After tumor establishment (day +15), mice received i.v. infusion of NT T cells or CAR.GD2 T cells (Supplementary Fig. S14A). While in the NT-T mice group, the bioluminescence of the tumor rapidly increased up to 3 logs in 40 days (Supplementary Fig. S14B and S14C), and mice either died or were sacrificed due to morbidity, mice receiving CAR.GD2 T cells experienced a longer tumor control, with a significantly lower bioluminescence signal (Supplementary Fig. S14B–S14D), translating into a significant prolongation of OS (Supplementary Fig. S14E, $P = 0.03$). Moreover, we observed a significant expansion of circulating T cells (CD45$^+$/CD3$^+$) in the PB of CAR.GD2 T-cell–treated mice as compared with control mice (Supplementary

Fig. S14F). The percentage of CAR$^+$ T cells remained stable up to the end of the experiment (day +58; Supplementary Fig. S14G). We also evaluated the *in vivo* longitudinal modulation of both CD4$^+$ and CD8$^+$ T cells in PB of treated mice, and we observed a significant CD8$^+$ T-cell enrichment and a CD4$^+$ T-cell decrease over time only in mice treated with CAR.GD2 T cells (Supplementary Fig. S15A and S15B). To evaluate the expression of GD2 in the tumor mass not fully eradicated by CAR.GD2 T cells, we have carried out a specific experiment as reported in Supplementary Fig. S14A but sacrificing the mice at day +46. We observed that in two mice (#4 and #5) treated with CAR.GD2 T cells, but in none of the mice receiving NT T cells, GD2 MFI was decreased compared with the expression of GD2 in the tumor mass of mice treated with NT T cells or in the tumor cell line evaluated before the infusion (Supplementary Fig. S15C and D). Notably, in mice #4 and #5 treated with CAR.GD2 T cells, we observed an elevated level of circulating CD3$^+$ cells, as well as of CAR$^+$ T cells (Supplementary Fig. S15E and S15F), and enhanced T-cell infiltration into the tumor (Supplementary Fig. S15G).

The iC9 suicide gene activation with AP1903 promotes CAR.GD2 T-cell eradication in the MB-PDX mouse model

Lastly, we sought to evaluate whether the systemic administration of AP1903 could induce a rapid elimination of both blood circulating and brain/MB-infiltrating CAR T cells by activating the iC9 suicide gene. To this aim, we developed an orthotopic PDX mouse model implanting Med-411FH mCherry/Luciferase cells. After tumor establishment (30 days), either NT T cells or CAR.GD2 T cells were infused i.v. (**Fig. 6A**). After 10 days from T-cell infusion, three mice in each cohort received i.p. the dimerizing agent AP1903, which activates iC9 for 3 consecutive days (day +11/day +12/day +13; **Fig. 6A**). As shown in **Fig. 6B** and C, AP1903 administration induced a significant reduction of circulating CD3$^+$ CAR$^+$ T cells [from 45.7% ± 9.27% pre-AP1903 (day +10) to 1.5% ± 2.29% post-AP1903 (day +14); P = 0.02, **Fig. 6C**]. NSG mice were sacrificed 24 hours from the last AP1903 administration (day +14) to characterize *ex vivo* the tumor T-cell infiltration. IHC analysis revealed CAR.GD2 T-cell infiltration into tumor sections (Supplementary Fig. S16), demonstrating their ability
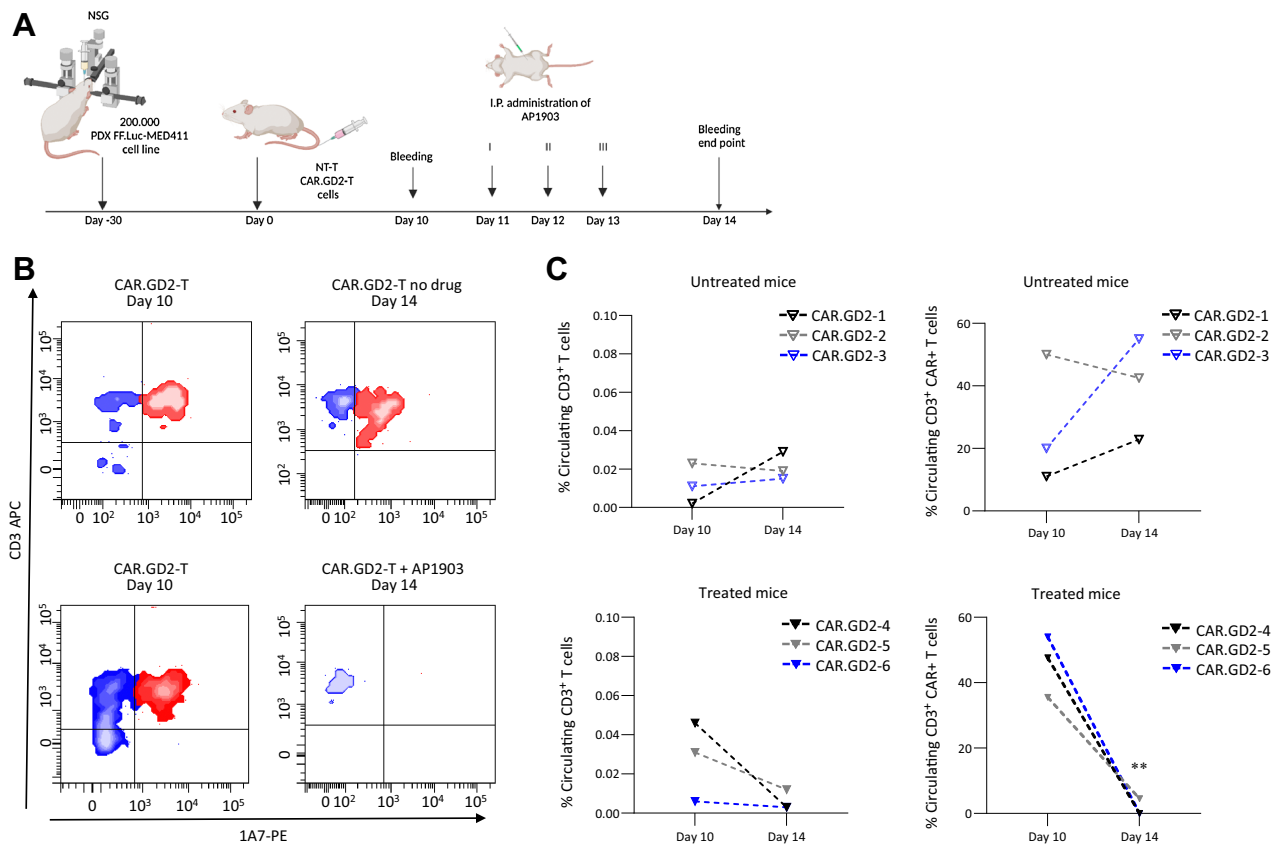

Figure 6.
iC9 activation by administration of AP1903 and the prompt decline of CAR.GD2 T cells from peripheral blood of the MB xenograft mice model. **A,** Illustration of experimental design in which Med-411 FH mCherry/Luc PDX cells were stereotaxically implanted into the cerebellum of 13 NSG mice. After 30 days from the tumor engraftment, 12 mice were infused with the effector T cells (six with CAR.GD2 T cells and six with NT T cells) through i.v. injection. On days 11, 12, and 13, mice (three out of six mice treated with NT T cells and three out of six mice treated with CAR.GD2 T cells) received three consecutive doses of the AP1903 dimerizing drug (100 μg/day/mouse). Flow-cytometry analysis of human T cells was performed on peripheral blood of the experimental mice one day before the AP1903 administration (day 10) and at the end of the experiment (day 14). **B,** AP1903 efficiently induces a strong reduction of circulating CAR.GD2 T cells. Plots depict CD3$^+$ and CAR$^+$ T-cell evaluation in exemplificative mice receiving CAR.GD2 T cells either untreated (no infusion of AP1903, top) or treated with AP1903 (bottom), on days 10 and 14. **C,** Flow-cytometry analysis of human CD3$^+$ T cells (left) or CAR$^+$ T cells (right) in MB-bearing mice receiving CAR. GD2 T cells untreated (top) and treated with AP1903 (bottom). One-way ANOVA was used as a multicomparison test. *, $P < 0.05$; **, $P < 0.01$; ***, $P < 0.001$; ****, $P < 0.0001$. (**A,** Created with BioRender.com.)

to cross the blood–brain barrier (BBB) and migrate into the tumor niche (Supplementary Fig. S16A), whereas in mice receiving NT T cells tumor-infiltrating T cells were not observed (Supplementary Fig. S17A and S17B). Moreover, the IHC analysis showed clearly the disappearance of infiltrating T cells in AP1903-treated mice, supporting the ability of AP1903 to both cross the BBB and eliminate tumor-infiltrating CAR.GD2 T cells (Supplementary Fig. S16 B).

Discussion

Recent preclinical and clinical studies have shown promising results associated with the use of CAR T-cell–based therapies for the treatment of cancer (14, 33). Although clinical trials based on anti-CD19.CAR T cells achieved unprecedented results for the treatment of B-cell malignancies (34), there is limited evidence of antitumor activity of CAR T cells in solid tumors. In particular, the identification of a suitable target antigen, highly expressed in solid tumors and with a restricted expression in normal tissues, represents a major limitation.

With respect to CNS tumors, recently it has been demonstrated that H3K27M-mutated diffuse intrinsic pontine glioma (DIPG) or spinal cord diffuse midline gliomas (DMG) unequivocally express GD2 antigen (14, 25, 46). Notably, the infusion of CAR.GD2 T cells in patients with H3K27M-mutated DIPG or spinal cord DMG has been reported to be associated mainly with toxicities related to the peculiar location of these tumors and manageable with intensive supportive care (14). Three of the 4 patients reported by the authors exhibited clinical and radiographic improvement after CAR.GD2 T-cell infusion.

Here, we report for the first time the evaluation of GD2 expression on a large number of pediatric patients affected by MB, generally recognized as a rare disease. GD2 was found to be overexpressed in the majority of MB cases at diagnosis, although with a large heterogeneity. Importantly, SHH and G3/G4 subgroups showed the highest GD2 expression, therefore making CAR.GD2 T cells a suitable immunotherapy approach for patients affected by these most aggressive MB subtypes. Indeed, in addition to the observed heterogeneity in GD2 expression on MB primary tissues, we provide evidence that CAR.GD2 T cells could provide benefit to control MB tumors, especially considering the lack of therapeutic options for patients with relapsed MB, and that it is possible to upregulate GD2 antigen on tumor cells by inhibiting the histone methyltransferase EZH2.

Our recent phase I/II clinical trial has shown promising results for both the safety profile and the therapeutic efficacy of CAR.GD2 T-cell therapy in neuroblastoma patients (33). In light of these premises, we hypothesized that GD2 could also be selected as tumor-associated antigen for MB patients and could be targeted by CAR.GD2 T cells. In our preclinical experiments on GD2$^+$ MB, we documented a significant antitumor activity of these CAR.GD2 T cells in MB both *in vitro* and *in vivo* models. In particular, CAR.GD2 T cells mediated a remarkable killing activity against GD2$^+$ MB cell lines and a MB-PDX model, as proved by the use of long-term coculture assay evaluating tumor control at the steady state of 5 days, or in real-time by the use of a live-cell imaging system. Indeed, monitoring cocultures between D283 Med or DAOY cell lines and CAR.GD2 T cells from the very early time point (1 hour) to the final point of evaluation (5 days), we observed a significant tumor control already evident at early time points. We also demonstrated that tumor recognition and elimination strictly depend on the level of antigen expression. Indeed, DAOY cells, which show a low GD2 MFI level,

were not fully eliminated in the *in vitro* models by CAR.GD2 T cells, with residual tumor cells characterized by an even lower GD2 MFI compared with cells incubated with control NT T cells.

Low expression of the target antigen on cancer cells is a well-known potential mechanism of resistance to CAR T-cell therapy. Recently, it has been reported in Ewing sarcoma (31), neuroblastoma (27), and lung cancers (15), that the EZH2 inhibitor tazemetostat, selectively and reversibly, induces GD2 surface expression without altering cell viability. However, inhibition of the histone methyltransferase EZH2 failed to increase GD2 expression in osteosarcoma cell lines (47). In a phase I/II trial (NCT01897571) for patients with advanced solid tumors, the recommended pediatric phase II dose of tazemetostat was determined to be 800 mg twice daily (48), with tolerable adverse events most frequently (>15%), including asthenia, anemia, anorexia, muscle spasms, nausea, and vomiting. In the context of MB, it was not foreseeable which effect this drug would have on the tumor itself, and for GD2 expression. Here, for the first time, we show that also in GD2low MB cell lines DAOY and MED-411 FHTC, GD2 expression can be upregulated after exposure to the EZH2 inhibitor tazemetostat, sensitizing tumor cells to the cytotoxic effect of CAR.GD2 T cells. Moreover, in our study, we demonstrated that tazemetostat treatment can cross the BBB and upregulate *in vivo* the GD2 expression on low–GD2-expressing MB cells (i.e., DAOY), sensitizing them to the lytic activity of CAR.GD2 T cells. This suggests a potential synergistic effect between tazemetostat and CAR.GD2 T cells in the context of MB.

However, despite these encouraging experimental data, further studies on *in vivo* models are needed to evaluate the optimal dose, time schedule, as well as route of administration for the combinatory use of tazemetostat and CAR.GD2 T cells, to reach the goal of complete tumor control, while preserving a favorable safety profile.

In order to better recapitulate the human pathophysiologic condition, we established three *in vivo* orthotopic mice models of MB. In line with our *in vitro* data, CAR.GD2 T cells were able to exert a significant control of tumor growth and, as a consequence, mice bearing MB tumors and treated with CAR.GD2 T cells showed a significantly prolonged OS as compared with mice receiving NT T cells.

Concerning the delivery route of CAR T cells, it is well known that this could significantly affect the response in patients affected by solid tumors, especially those suffering from CNS tumors (49). In our study, systemic i.v. delivery of CAR T cells was able to exert a significant antitumor response in the animal model of MB, being associated with a significantly better animal DFS and a high number of tumor-infiltrating T cells. Notably, it has been reported that the use of CAR T cells could induce fatal side effects, such as cytokine-release syndrome (CRS; refs. 34, 50) or neurologic toxicities (14, 36). Neurotoxicity is one of the most common and life-threatening complications of CAR T-cell therapy (34, 35). CAR T cells are known to cross and disrupt the BBB. It has been reported that a robust activation of anti–CD19-CAR T cells can induce fatal neurotoxicity associated with CAR T-cell trafficking into the CNS, due to endothelial activation and breakdown of the BBB (36), rather than an on-target/off-tumor effect. Two recent clinical trials provide important information about the safety profile of CAR.GD2 T-cell therapy. In a phase I/II clinical trial, although none of the 27 neuroblastoma patients treated with a third generation of CAR.GD2 T cells developed a central neurotoxic effect, most of them developed grade 1–2 cytokine-release syndrome (33). Moreover, 4 patients with H3K27M-mutated DIPG or spinal cord DMG, treated with second-generation CAR.GD2 T cells, although developing symptoms of on-tumor inflammation-associated

neurotoxicity, they did not show any signs or symptoms of on-target, off-tumor toxicity (14). However, considering the peculiar location of SNC tumors, neurotoxicity after CAR T-cell treatment needs to be seriously taken into consideration. For this reason, we have included in our construct the iC9 suicide gene, able to promptly eliminate the genetically modified T cells, as shown in several preclinical models and/or clinical setting (12, 33, 43, 51, 52). In this study, we have documented that the systemic administration of the dimerizing drug AP1903 led to the significant reduction of both circulating CAR.GD2 T cells and brain/tumor-infiltrating human CAR$^+$ T cells. Therefore, for a future clinical application of CAR.GD2 T cells in MB patients, the inclusion of a suicide gene may represent an additional safety mechanism to mitigate potential risks related to the therapy.

Conclusions

In conclusion, CAR.GD2 T cells show a strong *in vitro* and *in vivo* efficacy against MB cells. The suicide gene iC9 is able to increase the safety profile of the CAR.GD2 T-cell therapy, being able to eliminate CAR T cells that have crossed the BBB. Additionally, pretreatment with tazemetostat upregulates GD2 expression in MB tumor cells, sensitizing GD2^{dim}MB cells to the lytic effect displayed by CAR.GD2 T cells. These promising experimental results represent the basis for a phase I/II clinical trial to be conducted in patients with GD2$^+$ MB (NCT05298995).

Authors' Disclosures

C. Quintarelli reports a patent for 102023000011250 pending. B. De Angelis reports a patent for n. 102023000011250 pending. No disclosures were reported by the other authors.

Authors' Contributions

R. Ciccone: Data curation, formal analysis, investigation, methodology, writing–original draft. **C. Quintarelli:** Conceptualization, data curation, formal analysis, supervision, funding acquisition, validation, investigation, visualization, methodology, writing–review and editing. **A. Camera:** Visualization, methodology. **M. Pezzella:** Data curation, software, formal analysis, validation, investigation, visualization, methodology, writing–review and editing. **S. Caruso:** Data curation, formal analysis, investigation. **S. Manni:** Data curation, formal analysis, investigation, methodology. **A. Ottaviani:** Data curation, formal analysis, investigation, methodology. **M. Guercio:** Data curation, formal analysis, investigation, visualization, methodology. **F. Del Bufalo:** Data curation, formal analysis, investigation, visualization, methodology, writing–review and editing. **M.C. Quadraccia:** Data curation, formal analysis, investigation, visualization, methodology. **D. Orlando:** Investigation, visualization, methodology. **S. Di Cecca:** Data curation, investigation, visualization, methodology. **M. Sinibaldi:** Data curation, validation, investigation, methodology. **M. Aurigemma:** Investigation, visualization, methodology. **L. Iaffaldano:** Formal analysis, validation, investigation, visualization, methodology. **A. Sarcinelli:** Investigation, visualization, methodology. **M.L. D'Amore:** Formal analysis, visualization, methodology. **M. Ceccarelli:** Formal analysis, validation, investigation. **F. Nazio:** Funding acquisition, validation, investigation, visualization, methodology. **V. Marabitti:** Visualization, methodology. **E. Giorda:** Investigation, visualization, methodology. **M. Pezzullo:** Investigation, visualization, methodology. **C. De Stefanis:** Investigation, visualization, methodology. **A. Carai:** Validation, investigation, visualization, writing–review and editing. **S. Rossi:** Visualization, methodology. **R. Alaggio:** Visualization, methodology. **G. Del Baldo:** Formal analysis, validation, investigation, visualization, methodology. **M. Becilli:** Investigation, visualization, methodology. **A. Mastronuzzi:** Data curation, formal analysis, funding acquisition, visualization, methodology, writing–review and editing. **B. De Angelis:** Conceptualization, resources, data curation, formal analysis, supervision, funding acquisition, validation, investigation, visualization, methodology, writing–original draft, writing–review and editing. **F. Locatelli:** Conceptualization, formal analysis, funding acquisition, writing–review and editing.

Acknowledgments

Note

Supplementary data for this article are available at Clinical Cancer Research Online (http://clincancerres.aacrjournals.org/).

References

1. Maier H, Dalianis T, Kostopoulou ON. New approaches in targeted therapy for medulloblastoma in children. Anticancer Res 2021;41:1715–26.
2. Kumar V, Kumar V, McGuire T, Coulter DW, Sharp JG, Mahato RI. Challenges and recent advances in medulloblastoma therapy. Trends Pharmacol Sci 2017; 38:1061–84.
3. Louis DN, Perry A, Reifenberger G, von Deimling A, Figarella-Branger D, Cavenee WK, et al. The 2016 World Health Organization classification of tumors of the central nervous system: a summary. Acta Neuropathol 2016;131:803–20.
4. Northcott PA, Robinson GW, Kratz CP, Mabbott DJ, Pomeroy SL, Clifford SC, et al. Medulloblastoma. Nat Rev Dis Primers 2019;5:11.
5. Ribi K, Relly C, Landolt MA, Alber FD, Boltshauser E, Grotzer MA. Outcome of medulloblastoma in children: long-term complications and quality of life. Neuropediatrics 2005;36:357–65.
6. Jakacki RI, Burger PC, Zhou T, Holmes EJ, Kocak M, Onar A, et al. Outcome of children with metastatic medulloblastoma treated with carboplatin during craniospinal radiotherapy: a Children's Oncology Group Phase I/II study. J Clin Oncol 2012;30:2648–53.
7. Martin AM, Raabe E, Eberhart C, Cohen KJ. Management of pediatric and adult patients with medulloblastoma. Curr Treat Options Oncol 2014;15:581–94.
8. Baliga S, Gallotto S, Bajaj B, Lewy J, Weyman E, Lawell MP, et al. Decade-long disease, secondary malignancy, and brainstem injury outcomes in pediatric and young adult medulloblastoma patients treated with proton radiotherapy. Neuro Oncol 2022;24:1010–9.
9. Choi JY. Medulloblastoma: current perspectives and recent advances. Brain Tumor Res Treat 2023;11:28–38.
10. Clifford SC, Lusher ME, Lindsey JC, Langdon JA, Gilbertson RJ, Straughton D, et al. Wnt/Wingless pathway activation and chromosome 6 loss characterize a distinct molecular sub-group of medulloblastomas associated with a favorable prognosis. Cell Cycle 2006;5:2666–70.
11. Majzner RG, Mackall CL. Clinical lessons learned from the first leg of the CAR T cell journey. Nat Med 2019;25:1341–55.
12. Quintarelli C, Orlando D, Boffa I, Guercio M, Polito VA, Petretto A, et al. Choice of costimulatory domains and of cytokines determines CAR T-cell activity in neuroblastoma. Oncoimmunology 2018;7:e1433518.

13. Mount CW, Majzner RG, Sundaresh S, Arnold EP, Kadapakkam M, Haile S, et al. Potent antitumor efficacy of anti-GD2 CAR T cells in H3-K27M(+) diffuse midline gliomas. Nat Med 2018;24:572–9.

14. Majzner RG, Ramakrishna S, Yeom KW, Patel S, Chinnasamy H, Schultz LM, et al. GD2-CAR T cell therapy for H3K27M-mutated diffuse midline gliomas. Nature 2022;603:934–41.

15. Reppel L, Tsahouridis O, Akulian J, Davis IJ, Lee H, Fuca G, et al. Targeting disialoganglioside GD2 with chimeric antigen receptor-redirected T cells in lung cancer. J Immunother Cancer 2022;10.

16. Nazha B, Inal C, Owonikoko TK. Disialoganglioside GD2 expression in solid tumors and role as a target for cancer therapy. Front Oncol 2020;10:1000.

17. Esaki N, Ohkawa Y, Hashimoto N, Tsuda Y, Ohmi Y, Bhuiyan RH, et al. ASC amino acid transporter 2, defined by enzyme-mediated activation of radical sources, enhances malignancy of GD2-positive small-cell lung cancer. Cancer Sci 2018;109:141–53.

18. Mansoori M, Roudi R, Abbasi A, Abolhasani M., Abdi Rad I, Shariftabrizi A, et al. High GD2 expression defines breast cancer cells with enhanced invasiveness. Exp Mol Pathol 2019;109:25–35.

19. Theruvath J, Menard M, Smith BAH, Linde MH, Coles GL, Dalton GN, et al. Anti-GD2 synergizes with CD47 blockade to mediate tumor eradication. Nat Med 2022;28:333–44.

20. Longee DC, Wikstrand CJ, Mansson JE, He X, Fuller GN, Bigner SH, et al. Disialoganglioside GD2 in human neuroectodermal tumor cell lines and gliomas. Acta Neuropathol 1991;82:45–54.

21. Paret C, Ustjanzew A, Ersali S, Seidmann L, Jennemann R, Ziegler N, et al. GD2 expression in medulloblastoma and neuroblastoma for personalized immunotherapy: a matter of subtype. Cancers (Basel) 2022;14:6051.

22. Haydar D, Houke H, Chiang J, Yi Z, Ode Z, Caldwell K, et al. Cell-surface antigen profiling of pediatric brain tumors: B7-H3 is consistently expressed and can be targeted via local or systemic CAR T-cell delivery. Neuro Oncol 2021;23:999–1011.

23. Caforio M, Sorino C, Caruana I, Weber G, Camera A, Cifaldi L, et al. GD2 redirected CAR T and activated NK-cell-mediated secretion of IFNgamma overcomes MYCN-dependent IDO1 inhibition, contributing to neuroblastoma cell immune escape. J Immunother Cancer 2021;9:e001502.

24. Tumino N, Weber G, Besi F, Del Bufalo F, Bertaina V, Paci P, et al. Polymorphonuclear myeloid-derived suppressor cells impair the anti-tumor efficacy of GD2.CAR T-cells in patients with neuroblastoma. J Hematol Oncol 2021;14:191.

25. de Billy E, Pellegrino M, Orlando D, Pericoli G, Ferretti R, Businaro P, et al. Dual IGF1R/IR inhibitors in combination with GD2-CAR T-cells display a potent anti-tumor activity in diffuse midline glioma H3K27M-mutant. Neuro Oncol 2022;24:1150–63.

26. Majzner RG, Mackall CL. Tumor antigen escape from CAR T-cell therapy. Cancer Discov 2018;8:1219–26.

27. Mabe NW, Huang M, Dalton GN, Alexe G, Schaefer DA, Geraghty AC, et al. Transition to a mesenchymal state in neuroblastoma confers resistance to anti-GD2 antibody via reduced expression of ST8SIA1. Nat Cancer 2022;3:976–93.

28. Nguyen K, Yan Y, Yuan B, Dasgupta A, Sun J, Mu H, et al. ST8SIA1 regulates tumor growth and metastasis in TNBC by activating the FAK-AKT-mTOR signaling pathway. Mol Cancer Ther 2018;17:2689–701.

29. Muller J, Hart CM, Francis NJ, Vargas ML, Sengupta A, Wild B, et al. Histone methyltransferase activity of a Drosophila Polycomb group repressor complex. Cell 2002;111:197–208.

30. Czermin B, Melfi R, McCabe D, Seitz V, Imhof A, Pirrotta V. Drosophila enhancer of Zeste/ESC complexes have a histone H3 methyltransferase activity that marks chromosomal Polycomb sites. Cell 2002;111:185–96.

31. Kailayangiri S, Altvater B, Lesch S, Balbach S, Gottlich C, Kuhnemundt J, et al. EZH2 inhibition in Ewing sarcoma upregulates G(D2) expression for targeting with gene-modified T cells. Mol Ther 2019;27:933–46.

32. Louis CU, Savoldo B, Dotti G, Pule M, Yvon E, Myers GD, et al. Antitumor activity and long-term fate of chimeric antigen receptor-positive T cells in patients with neuroblastoma. Blood 2011;118:6050–6.

33. Del Bufalo F, De Angelis B, Caruana I, Del Baldo G, De Ioris MA, Serra A, et al. GD2-CART01 for relapsed or refractory high-risk neuroblastoma. N Engl J Med 2023;388:1284–95.

34. Brudno JN, Kochenderfer JN. Recent advances in CAR T-cell toxicity: mechanisms, manifestations and management. Blood Rev 2019;34:45–55.

35. Gust J, Ponce R, Liles WC, Garden GA, Turtle CJ. Cytokines in CAR T cell-associated neurotoxicity. Front Immunol 2020;11:577027.

36. Gust J, Hay KA, Hanafi LA, Li D, Myerson D, Gonzalez-Cuyar LF, et al. Endothelial activation and blood-brain barrier disruption in neurotoxicity after adoptive immunotherapy with CD19 CAR-T cells. Cancer Discov 2017; 7:1404–19.

37. Gargett T, Brown MP. The inducible caspase-9 suicide gene system as a "safety switch" to limit on-target, off-tumor toxicities of chimeric antigen receptor T cells. Front Pharmacol 2014;5:235.

38. Tran S, Bielle F. WHO 2021 and beyond: new types, molecular markers and tools for brain tumor classification. Curr Opin Oncol 2022;34:670–5.

39. Ivanov DP, Coyle B, Walker DA, Grabowska AM. In vitro models of medulloblastoma: choosing the right tool for the job. J Biotechnol 2016; 236:10–25.

40. Zeytin HE, Tripathi PK, Bhattacharya-Chatterjee M, Foon KA, Chatterjee SK. Construction and characterization of DNA vaccines encoding the single-chain variable fragment of the anti-idiotype antibody 1A7 mimicking the tumor-associated antigen disialoganglioside GD2. Cancer Gene Ther 2000;7: 1426–36.

41. De Matteis S, Dicataldo M, Casadei B, Storci G, Laprovitera N, Arpinati M, et al. Peripheral blood cellular profile at pre-lymphodepletion is associated with CD19-targeted CAR-T cell-associated neurotoxicity. Front Immunol 2022;13: 1058126.

42. Di Stasi A, De Angelis B, Savoldo B. Gene therapy to improve migration of T cells to the tumor site. Methods Mol Biol 2010;651:103–18.

43. Orlando D, Miele E, De Angelis B, Guercio M, Boffa I, Sinibaldi M, et al. Adoptive immunotherapy using PRAME-specific T cells in medulloblastoma. Cancer Res 2018;78:3337–49.

44. Kurmasheva RT, Sammons M, Favours E, Wu J, Kurmashev D, Cosmopoulos K, et al. Initial testing (stage 1) of tazemetostat (EPZ-6438), a novel EZH2 inhibitor, by the pediatric preclinical testing program. Pediatr Blood Cancer 2017;64: 10.1002/pbc.26218.

45. Schoeberl F, Tiedt S, Schmitt A, Blumenberg V, Karschnia P, Burbano VG, et al. Neurofilament light chain serum levels correlate with the severity of neurotoxicity after CAR T-cell treatment. Blood Adv 2022;6:3022–6.

46. Gargett T, Ebert LM, Truong NTH, Kollis PM, Sedivakova K, Yu W, et al. GD2-targeting CAR-T cells enhanced by transgenic IL-15 expression are an effective and clinically feasible therapy for glioblastoma. J Immunother Cancer 2022;10: e005187.

47. Wiebel M, Kailayangiri S, Altvater B, Meltzer J, Grobe K, Kupich S, et al. Surface expression of the immunotherapeutic target G(D2) in osteosarcoma depends on cell confluency. Cancer Rep (Hoboken) 2021;4:e1394.

48. Italiano A, Soria JC, Toulmonde M, Michot JM, Lucchesi C, Varga A, et al. Tazemetostat, an EZH2 inhibitor, in relapsed or refractory B-cell non-Hodgkin lymphoma and advanced solid tumours: a first-in-human, open-label, phase 1 study. Lancet Oncol 2018;19:649–59.

49. Prapa M, Chiavelli C, Golinelli G, Grisendi G, Bestagno M, Di Tinco R, et al. GD2 CAR T cells against human glioblastoma. NPJ Precis Oncol 2021;5:93.

50. Frey N, Porter D. Cytokine release syndrome with chimeric antigen receptor T cell therapy. Biol Blood Marrow Transplant 2019;25:e123–e7.

51. Guercio M, Manni S, Boffa I, Caruso S, Di Cecca S, Sinibaldi M, et al. Inclusion of the inducible caspase 9 suicide gene in CAR construct increases safety of CAR.CD19 T cell therapy in B-cell malignancies. Front Immunol 2021;12:755639.

52. Guercio M, Orlando D, Di Cecca S, Sinibaldi M, Boffa I, Caruso S, et al. CD28. OX40 co-stimulatory combination is associated with long in vivo persistence and high activity of CAR.CD30 T-cells. Haematologica 2021;106:987–99.